Journal of Thermal Science Vol.31, No.6 (2022) 2051−2067

https://doi.org/10.1007/s11630-022-1677-7 **Article ID: 1003-2169(2022)06-2051-17**

Performance Analysis of an Integrated Supercritical CO_2 Recompression/ Absorption Refrigeration/Kalina Cycle Driven by Medium-Temperature Waste Heat

SU Ruizhi[1,2], YU Zeting[1,2*], WANG Daohan[3], SUN Bo[4], SUN Jia'nan[1,2]

1. School of Energy and Power Engineering, Shandong University, Ji'nan 250061, China
2. Shandong Engineering Laboratory for High-Efficiency Energy Conservation and Energy Storage Technology & Equipment, Shandong University, Ji'nan 250061, China
3. School of Electrical Engineering, Shandong University, Ji'nan 250061, China
4. School of Control Science and Engineering, Shandong University, Ji'nan 250061, China

Abstract: A novel power and cooling cogeneration system which combines a supercritical CO_2 recompression cycle (SCRC), an ammonia-water absorption refrigeration cycle (AARC) and a Kalina cycle (KC) is proposed and investigated for the recovery of medium-temperature waste heat. The system is based on energy cascade utilization, and the waste heat can be fully converted through the simultaneous operation of the three sub-cycles. A steady-state mathematical model is built for further performance study of the proposed system. When the exhaust temperature is 505°C, it is shown that under designed conditions the thermal efficiency and exergy efficiency reach 30.74% and 61.55%, respectively. The exergy analysis results show that the main exergy destruction is concentrated in the heat recovery vapor generator (HRVG). Parametric study shows that the compressor inlet pressure, the SCRC pressure ratio, the main compressor and the turbine I inlet temperature, and the AARC generator pressure have significant effects on thermodynamic and economic performance of the combined system. The findings in this study could provide guidance for system design to achieve an efficient utilization of medium-temperature waste heat (e.g., exhaust heat from gas turbine, high-temperature fuel cells and internal combustion engine).

Keywords: waste heat utilization, cogeneration system, supercritical CO_2 recompression cycle, absorption refrigeration cycle, Kalina cycle

1. Introduction

With the continuous growth of energy demand and over-exploitation of fossil fuels, the effective utilization of waste heat from industrial processes has become an important measure for energy-saving and emission-reduction. According to the temperature level, the waste heat sources can be divided into low-temperature (<230°C), medium-temperature (230°C–650°C), and high-temperature (>650°C) resources [1]. Among them, the medium-temperature waste heat resource has the characteristics of easy utilization, mature conversion

Received: Mar 01, 2020 AE: PENG Jingqing Corresponding author: YU Zeting E-mail: yuzt@sdu.edu.cn

Nomenclature		**Subscripts**	
A	heat transfer area/m^2	abs	absorber
C	purchased cost/USD	c	cooling
CRF	capital recovery factor	ci	capital investment
COP	coefficient of performance	comp	compressor
E	exergy rate/kW	cond	condenser
h	specific enthalpy/$kJ \cdot kg^{-1}$	ex	exergy
I	exergy destruction/kW	eva	evaporator
j	interest rate	g	gas
m	mass flow rate/$kg \cdot s^{-1}$	gen	generator
N	annual operational hours/h	h	heating
P	pressure/MPa	in	input
PR	pressure ratio	max	maximum
Q	heat transfer rate/kW	min	minimum
s	specific entropy/$kJ \cdot kg^{-1} \cdot K^{-1}$	net	net
T	temperature/°C	om	operating and maintenance
U	overall heat-transfer coefficient/$W \cdot m^{-2} \cdot K^{-1}$	out	output
W	power rate/kW	rec	rectifier
x	ammonia mass concentration	s	isentropic progress
ε	effectiveness	th	first law
η	efficiency	tot	total
χ	recompression ratio	tur	turbine

technology and wide sources (such as industrial waste heat, engine exhaust gases, fuel cells and combined gas cycles, etc.). Therefore, the efficient recovery of medium-temperature waste heat has a great significance to the sustainable development of the world [2–4]. Sadreddini et al. [5] proposed a novel cascade transcritical CO_2 and ORC cycle to recover medium-temperature waste heat, and liquefied natural gas (LNG) was used as heat sink. They found the performance of the new cascade cycle is better than the single cycles. Mohtaram et al. [6] used a recuperative ammonia-water system to recover the medium-temperature waste heat from gas turbine exhaust, and the effects of compressor pressure ratio on the system thermodynamic performance was investigated. They also evaluated the effects of the dilution pressure and density of ammonia-water solutions on the combined system performance [7].

Furthermore, many studies paid attention on the utilization of medium-temperature waste heat with three commonly used cycles: steam Rankine cycles (SRCs), Kalina cycles (KCs), and organic Rankine cycles (ORCs) [8–10]. SRC has a history of more than 100 years, but in practical engineering applications, due to the fact that the thermodynamic performance of water used as working fluid will be limited by waste heat scale. This technology does not perform well in system efficiency, maintenance and economics [11]. ORC uses low-boiling organics as working fluid. However, most of the organics are toxic and its leakage is inevitable, and the investment cost for the working fluid is typically high [12]. KC can get a good temperature matching in the heat transfer processes with a non-zeotropic mixture of ammonia-water as the working fluid, but its applicable heat source temperature is usually below 400°C due to the corrosiveness of ammonia [13, 14].

Compared with the working fluids of water for SRC, organics for ORC and ammonia-water for KC, CO_2 has the advantages of low critical point, high stability, cost effective, environmentally friendly and wide sources, etc. The supercritical CO_2 (S-CO_2) power cycle has attracted the worldwide attention in the past few years due to its high power generation capacity [15, 16]. Furthermore, it has been proven that using recompression can achieve a higher energy conversion efficiency which is generally suitable for heat sources above 400°C [17], and many efforts have been made for the cycle waste heat utilization before it is rejected in the cooler [18–20]. Wang et al. [21] conducted a study of combining a S-CO_2 recompression cycle (SCRC) with a transcritical CO_2 (T-CO_2) cycle, and carried out a detailed thermodynamic and exergoeconomic analysis. They concluded that not only the combined cycle energy and exergy efficiency was achieved higher than SCRC, but also the cycle exergoeconomic performance was improved. Hou et al.

[22] proposed to use ORC as the bottom cycle to recover waste heat from SCRC, and the comparison analysis revealed the thermal and exergoeconomic superiorities of the combined system to the single SCRC and basic ORC. Li et al. [23] integrated SCRC with a KC, and the genetic algorithm was employed to optimize the SCRC/KC system performance. The result showed that the exergy efficiency and the total product unit cost of the combined cycle were 8.02% higher and 5.50% lower than the stand-along SCRC, and the exergy destruction cost rate and exergy destruction were reduced by 8.57% and 9.75%, respectively. Wu et al. [24] combined SCRC with an ammonia-water absorption chiller and performed an analysis for the novel system. They found that the first and second law efficiency both increased after combining SCRC with the refrigeration sub-system. Then Li et al. [25] proposed a SCRC/LiBr-H_2O system with lithium bromide-water as working fluid, and conducted a comparative study between this system and SCRC/AARC system. The result showed that the COP of SCRC/LiBr-H_2O system was higher than SCRC/AARC system, and SCRC/LiBr-H_2O system was easier to reach the balance between cooling and power. However, the range of evaporating temperature of LiBr-H_2O refrigeration cycle was very narrow in order to prevent water from freezing, but ammonia didn't have this problem, and it could even evaporate at a temperature as low as –60°C [26]. Meanwhile, AARC could be driven by the heat source with a wider temperature range generally at 50–200°C than that of heat source driving the LiBr-H_2O refrigeration cycle [27].

When the waste heat is absorbed by SCRC, due to its high absorption temperature, the outlet waste heat temperature is still high which is also worth utilizing. From previous studies, it was known that Kalina cycle had many advantages in the recovery of low and medium-temperature waste heat [28–31]. For the utilization of low temperature geothermal water, Li et al. [32] found that KC presented a better economic performance and a higher thermal efficiency than transcritical CO_2 cycle, and Campos Rodríguez et al. [33] proved that KC also performed better than ORC. For the medium-temperature waste heat from Diesel engine, Bombarda et al. [34] got the conclusion that KC and ORC produced almost equal power outputs, and Jonsson et al. [35] found that KC was more efficient than the single and dual pressure steam cycle.

By reviewing the research mentioned above, it can be realized that the research on innovative and efficient combined systems for medium-temperature waste heat utilization has bright development prospects. There have been many studies about SCRC and its combined cycles for high-temperature waste heat, like nuclear reactor, whose temperature was high even reaching 850°C [36]. However, few studies focused on the performance of SCRC combined systems in the utilization of medium-temperature waste heat resources. And there has not been a study on the use of SCRC and KC to simultaneously recover medium-temperature waste heat based on the principle of energy cascade utilization. In this paper, for the purpose of fully recycling medium-temperature waste heat, a novel power and cooling cogeneration system integrated with a SCRC system, an AARC system and a KC system is proposed and investigated. The proposed system is designed for the medium-temperature waste heat above 400°C due to the existence of SCRC. The first recovery unit is SCRC. After the waste heat temperature decreases, it is suitable for KC, and the AARC serves as a bottom cycle to deeply recover the exhausted heat from SCRC. The coordinated operation of the three sub-systems greatly improves the waste heat recovery and conversion efficiency. To investigate the cogeneration system, a mathematical model is first developed, and then a parametric analysis is carried out to explore the impacts of some key parameters on the system performance. The findings could help to extend the utilization of medium-temperature waste heat and enhance the SCRC performance.

2. System Description

Fig. 1 illustrates the schematic of the proposed combined system (SCRC/AARC/KC). The system consists of three subsystems: a SCRC subsystem, an AARC subsystem and a KC subsystem. In the SCRC subsystem, the working fluid at the inlet of HTR (3) consists of two parts: one is from RC (3b), and the other is from MC and preheated by LTR (3a). Then the working fluid (4) is heated through the heater and produce power in turbine I. After the exhaust flows through HTR and LTR (7-8), the fluid again splits into two parts (8a and 8b), of which stream 8a directly provides energy for the bottom AARC.

In the AARC subsystem, the solution from the solution heat exchanger (SHX) (12) gains heat from stream 8a in the generator. A high concentration ammonia vapor is produced (16) and then it flows into the rectifier to get a higher concentration (18). Then the vapor is condensed to a saturated liquid state (19) by cooling water in condenser. The condensed liquid is further cooled by the pre-cooler (20), then it is depressurized by throttle valve I and enters the evaporator (21), where the refrigerant evaporates and produces cooling capacity for users. Meanwhile, after rejecting heat in SHX, the cooled solution (13) is throttled through valve II. Then it mixes with the pre-cooler outlet working fluid (23) in absorber I. The

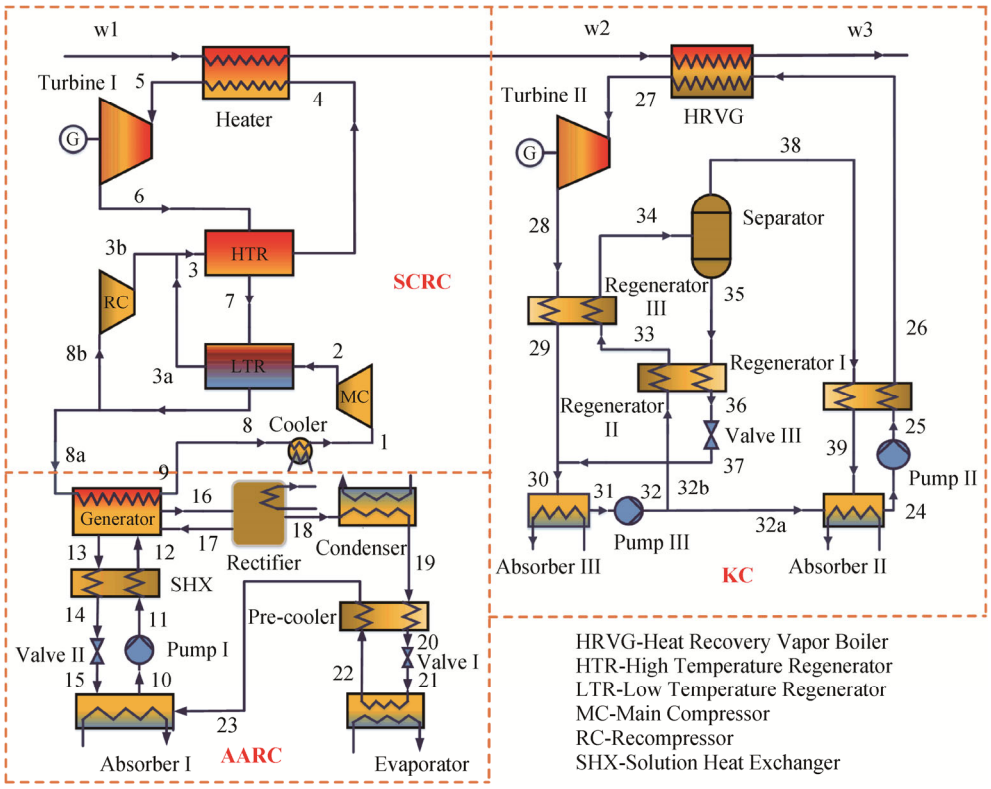

Fig. 1 Schematic of the proposed SCRC/AARC/KC system

mixed fluids are then cooled and pumped to SHX to complete the cycle.

In the KC subsystem, the ammonia-water solution at the outlet of absorber III (31) is pressurized by pump III and divided into two parts: stream 32a and 32b. Stream 32a directly enters absorber II. Stream 32b is heated by regenerator II and regenerator III, then enters the separator to separate high concentration vapor (38) and low concentration liquid (35). The ammonia vapor is mixed with stream 32a and pressurized by pump II. The mixed stream gains heat from the ammonia vapor in regenerator I and enters HRVG to further absorb exhaust heat (w2), and then the vapor expands in turbine II to produce power. The ammonia liquid (35) is depressurized by throttle valve III after exchanging heat in regenerator II, and then mixed with the working fluid from regenerator III (29) in absorber III to complete the cycle.

3. Mathematical Modeling

In this study, in order to simplify analysis, the following assumptions are employed for the combined system [37–41].

(1) The system operates at a steady state, and the changes in kinetic and potential energy are negligible.

(2) The heat losses and pressure drops of the system are neglected.

(3) The isentropic efficiency is employed in pumps, compressors and turbines.

(4) The liquid working fluids at the outlet of absorbers, condenser, rectifier, and separator are all saturated, and the vapors at the outlet of rectifier and separator are both saturated.

3.1 SCRC model

For the heater, the energy balance is given by

$$m_4\left(h_5-h_4\right)=m_{\mathrm{w}}\left(h_{\mathrm{w1}}-h_{\mathrm{w2}}\right) \tag{1}$$

For the high and low temperature regenerators, the heat balance equations are described as

$$m_6\left(h_6-h_7\right)=m_3\left(h_4-h_3\right) \tag{2}$$

$$m_7\left(h_7-h_8\right)=m_2\left(h_{3\mathrm{a}}-h_2\right) \tag{3}$$

For compressor, the isentropic efficiency is shown as

$$\eta_{\mathrm{c}}=\frac{h_{\mathrm{out,s}}-h_{\mathrm{in}}}{h_{\mathrm{out}}-h_{\mathrm{in}}} \tag{4}$$

The power consumption of main compressor (MC) and recompressor (RC) can be respectively shown as

$$W_{\mathrm{MC}}=m_1\left(h_2-h_1\right) \tag{5}$$

$$W_{\mathrm{RC}}=m_{8\mathrm{b}}\left(h_{3\mathrm{b}}-h_{8\mathrm{b}}\right) \tag{6}$$

For turbine, the isentropic efficiency is given by

$$\eta_{\mathrm{t}}=\frac{h_{\mathrm{in}}-h_{\mathrm{out,s}}}{h_{\mathrm{in}}-h_{\mathrm{out}}} \tag{7}$$

The power generated by turbine I is expressed by

$$W_{\text{turI}} = m_5\left(h_5 - h_6\right) \tag{8}$$

For the cooler, the energy balance is shown as

$$Q_{\text{cooler}} = m_9\left(h_9 - h_1\right) \tag{9}$$

The recompression ratio is defined as

$$\chi = \frac{m_{8\text{b}}}{m_8} \tag{10}$$

3.2 AARC model

For the generator, the energy balance is given by

$$m_{8\text{a}}\, h_{8\text{a}} - m_9\, h_9 = m_{13}\, h_{13} + m_{16} h_{16} - m_{12}\, h_{12} - m_{17}\, h_{17} \tag{11}$$

The ammonia mass conservation in the generator is described as

$$m_{12} + m_{17} = m_{13} + m_{16} \tag{12}$$

$$m_{12}x_{12} + m_{17}x_{17} = m_{13}x_{13} + m_{16}x_{16} \tag{13}$$

In the rectifier, the energy balance is given by

$$m_{16}h_{16} = m_{17}h_{17} + m_{18}h_{18} + Q_{\text{rec}} \tag{14}$$

The mass balance equation for rectifier is expressed as

$$m_{16} = m_{17} + m_{18} \tag{15}$$

$$m_{16}x_{16} = m_{17}x_{17} + m_{18}x_{18} \tag{16}$$

For absorber I, the energy balance is given by

$$m_{10}h_{10} + Q_{\text{absI}} = m_{15}h_{15} + m_{23}h_{23} \tag{17}$$

The mass conservation in absorber I is shown as

$$m_{10} = m_{15} + m_{23} \tag{18}$$

$$m_{10}x_{10} = m_{15}x_{15} + m_{23}x_{23} \tag{19}$$

For pump, the isentropic efficiency is expressed as

$$\eta_{\text{p}} = \frac{h_{\text{out,s}} - h_{\text{in}}}{h_{\text{out}} - h_{\text{in}}} \tag{20}$$

The power consumed by pump I is described as

$$W_{\text{pumpI}} = m_{10}\left(h_{11} - h_{10}\right) \tag{21}$$

The energy balance equation in SHX is given by

$$m_{11}h_{11} + m_{13}h_{13} = m_{12}h_{12} + m_{14}h_{14} \tag{22}$$

For the pre-cooler, the heat balance equation is described as

$$m_{19}h_{19} + m_{22}h_{22} = m_{20}h_{20} + m_{23}h_{23} \tag{23}$$

For the condenser, the energy balance is given by

$$Q_{\text{cond}} = m_{18}\left(h_{18} - h_{19}\right) \tag{24}$$

For the evaporator, the energy balance is shown as

$$Q_{\text{eva}} = m_{21}\left(h_{22} - h_{21}\right) \tag{25}$$

3.3 KC model

In the KC system, HRVG as an important heat exchange component consists of an economizer, an evaporator and a superheater. Unlike a single working fluid such as water, the evaporation process of ammonia-water mixture is completed under "variable temperature" conditions, which effectively reduces the heat transfer temperature difference. In this study, the ammonia solution experience a process from subcooled region to superheated region in the HRVG which is shown in Fig. 2, where T_{a} is ammonia-water temperature at economizer outlet; T_{d} is outlet exhaust heat temperature of evaporator.

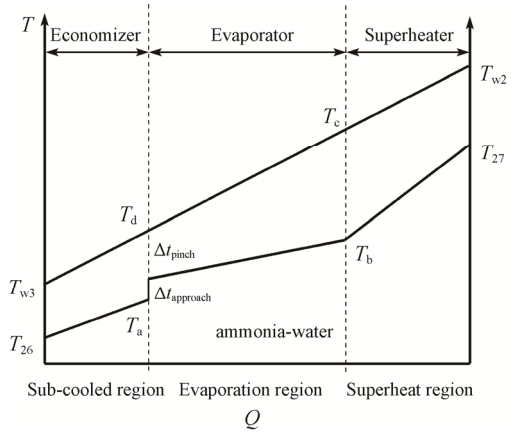

Fig. 2 Temperature profile in HRVG [39]

The heat balances equation in HRVG are expressed as follows [42]:

For the sub-cooled phase

$$m_{\text{w}}\left(h_{\text{d}} - h_{\text{w3}}\right) = m_{26}\left(h_{\text{a}} - h_{26}\right) \tag{26}$$

For the evaporation phase

$$m_{\text{w}}\left(h_{\text{c}} - h_{\text{d}}\right) = m_{26}\left(h_{\text{b}} - h_{\text{a}}\right) \tag{27}$$

For the superheated phase

$$m_{\text{w}}\left(h_{\text{w2}} - h_{\text{c}}\right) = m_{27}\left(h_{27} - h_{\text{b}}\right) \tag{28}$$

For all the regenerators, the energy balance can be described as

$$m_{\text{h}}(h_{\text{in,h}} - h_{\text{out,h}}) = m_{\text{c}}(h_{\text{out,c}} - h_{\text{in, c}}) \tag{29}$$

The power consumed by pump II and pump III is expressed by

$$W_{\text{pumpII}} = m_{24}\left(h_{25} - h_{24}\right) \tag{30}$$

$$W_{\text{pumpIII}} = m_{31}\left(h_{32} - h_{31}\right) \tag{31}$$

The power generated by turbine II is shown as

$$W_{\text{turII}} = m_{27}\left(h_{27} - h_{28}\right) \tag{32}$$

Similarly, all components must meet the law of mass conservation, which can be expressed as

$$\sum m_{\text{in}} - \sum m_{\text{out}} = 0 \tag{33}$$

$$\sum m_{\text{in}}\, x_{\text{in}} - \sum m_{\text{out}}\, x_{\text{out}} = 0 \tag{34}$$

3.4 Exergy analysis

In the process of reaching equilibrium with the environment, the maximum useful work that energy can transform is defined as exergy. Exergy analysis can

reflect the actual utilization share of energy and reveal where the system's exergy destruction mainly exists, and can provide an important reference for system improvement [43, 44].

The exergy not considering the chemical reactions is called physical exergy, which means the maximum possible work when a thermal system changes from a specified state to the environmental state through a reversible process, and the physical exergy of steady flow can be expressed as [45]

$$E_i = m_i\left[h_i - h_0 - T_0\left(s_i - s_0\right)\right] \tag{35}$$

The exergy balance equation is shown as

$$\sum E_{\text{in}} - \sum E_{\text{out}} - W_{\text{u}} - I = 0 \tag{36}$$

where W_{u} is the external output work or input work.

3.5 Economic analysis

Economic indicator is very important for system evaluation. Achieving a small investment cost is also one of the goals pursued in system design. In this study, all heat exchange components are taken as simple types whose size can be calculated by log Mean Temperature Difference (LMTD) methods. The amount of heat transfer in each heat exchange component is expressed as

$$Q_i = U_i\, A_i\, \Delta T_{\text{m}} \tag{37}$$

In Eq. (37), U_i represents the heat transfer coefficient, and the approximate values for each component are listed in Table 1. A_i is the heat transfer area, and ΔT_{m} is the logarithmic mean temperature difference which can be described as

$$\Delta T_{\text{m}} = \frac{\Delta T_{\max} - \Delta T_{\min}}{\ln\dfrac{\Delta T_{\max}}{\Delta T_{\min}}} \tag{38}$$

The cost of purchasing heat exchangers is influenced by the heat exchange area. For the pre-cooler, regenerator, HTR, LTR, and SHX, the correlation is [48]:

Table 1 Heat transfer coefficient (U_i) of system components [33, 46, 47]

Component	U_i/W·m^{-2}·°C^{-1}
Heater	1000
HRVG	900
HTR & LTR	1000
Generator	1600
Rectifier	1100
Condenser	1100
Cooler & Pre-cooler	1000
Evaporator	900
Absorber	600
Regenerator & SHX	1000

$$C = 130\left(\frac{A}{0.093}\right)^{0.78} \tag{39}$$

For the other heat exchangers, the correlations are shown in Table 2.

Table 2 Purchased equipment cost of system components [20, 48, 49]

Component	Purchase cost/USD
Heater	$C_{\text{heater}} = 17\,500\,(A_{\text{heater}}/100)^{0.6}$
HRVG	$C_{\text{HRVG}} = 17\,500\,(A_{\text{HRVG}}/100)^{0.6}$
Generator	$C_{\text{gen}} = 17\,500\,(A_{\text{gen}}/100)^{0.6}$
Cooler	$C_{\text{cooler}} = 8000(A_{\text{cooler}}/100)^{0.6}$
Rectifier	$C_{\text{rec}} = 17\,000(A_{\text{rec}}/100)^{0.6}$
Condenser	$C_{\text{cond}} = 8000(A_{\text{cond}}/100)^{0.6}$
Evaporator	$C_{\text{eva}} = 16\,000(A_{\text{eva}}/100)^{0.6}$
Absorber	$C_{\text{abs}} = 16\,500(A_{\text{abs}}/100)^{0.6}$

For MC and RC, the capital cost can be described as [20]

$$C_{\text{comp}} = 71.1 m_{\text{c}} \frac{1}{0.93 - \eta_{\text{c}}} \text{PR}\ln(\text{PR}) \tag{40}$$

For turbine I, the capital cost can be expressed as [23]

$$C_{\text{turI}} = 479.34 m_5 \frac{1}{0.92 - \eta_{\text{t}}} \times \text{PR}\ln(\text{PR})\left[1 + \exp\left(0.036T_5 - 54.4\right)\right] \tag{41}$$

For turbine II, the correlation is different from Eq. (41) due to the different kind of working fluids, which is given by [50]

$$\lg C_{\text{turII}} = 2.6259 + 1.4398\lg\left(W_{\text{turII}}\right) - 0.1776\left[\lg\left(W_{\text{turII}}\right)\right]^2 \tag{42}$$

For pumps, the capital cost is calculated by [33]

$$\lg C_{\text{pump}} = 3.3892 + 0.0536\lg\left(W_{\text{pump}}\right) + 0.1538\left[\lg\left(W_{\text{pump}}\right)\right]^2 \tag{43}$$

The purchase cost of other low-cost equipment such as the connecting pipes and the throttle valves is relative low that can be neglected in this study. Thus the total capital investment cost can be described as

$$C_{\text{ci}} = \sum C_i \tag{44}$$

The system operating and maintenance cost can be expressed as a weighted function of the capital investment cost, and the system total cost can be expressed as the sum of the two kinds of cost. The corresponding equations are shown as follows

$$C_{\text{om}} = \gamma C_{\text{ci}} \tag{45}$$

$$C'_{\text{tot}} = C_{\text{ci}} + C_{\text{om}} \tag{46}$$

where the weighting coefficient γ is set to 0.06 [24].

The system cost per unit time is defined as

$$C_{\text{tot}} = \frac{C'_{\text{tot}} \times \text{CRF}}{N} \tag{47}$$

where N represents the system annual operating time assumed as 8000 h [51], and CRF is the capital recovery factor defined as [52]

$$\text{CRF} = \frac{i_{\text{eff}}\left(1+i_{\text{eff}}\right)^n}{\left(1+i_{\text{eff}}\right)^n - 1} \tag{48}$$

In Eq. (48), i_{eff} is the annual interest rate and n represents the average service life, which are set to 6% and 20 years, respectively [48].

4. Performance Criteria

This combined system outputs two different forms of energy: electrical energy and cold energy. The net power output can be described as

$$W_{\text{net}} = \sum W_{\text{tur}} - \sum W_{\text{comp}} - \sum W_{\text{pump}} \tag{49}$$

The refrigeration output is equal to the heat amount transferred in the evaporator.

$$Q_{\text{c}} = Q_{\text{eva}} \tag{50}$$

The thermal efficiency of the combined cycle based on the first law of thermodynamics can be expressed as

$$\eta_{\text{th}} = \frac{W_{\text{net}} + Q_{\text{c}}}{Q_{\text{in}}} \tag{51}$$

We can use the first law efficiency on the three sub-cycles to evaluate their respective thermodynamic performance.

For SCRC, the net power output is given by

$$W_{\text{net,SCRC}} = W_{\text{turI}} - W_{\text{MC}} - W_{\text{RC}} \tag{52}$$

And the first law efficiency is

$$\eta_{\text{th,SCRC}} = \frac{W_{\text{net,SCRC}}}{Q_{\text{in,SCRC}}} \tag{53}$$

For KC, the net power output is given by

$$W_{\text{net,KC}} = W_{\text{turII}} - W_{\text{pumpII}} - W_{\text{pumpIII}} \tag{54}$$

And the first law efficiency is

$$\eta_{\text{th,KC}} = \frac{W_{\text{net,KC}}}{Q_{\text{in,KC}}} \tag{55}$$

AARC is a reverse cycle that can be evaluated using coefficient of performance (COP), which is defined as

$$\text{COP} = \frac{Q_{\text{c}}}{Q_{\text{in,gen}} + W_{\text{pumpI}}} \tag{56}$$

Based on the second law of thermodynamics, the system exergy efficiency is given by

$$\eta_{\text{ex}} = \frac{W_{\text{net}} + E_{\text{c}}}{E_{\text{in}}} \tag{57}$$

where E_{c} is the system cold exergy output, which can be expressed as

$$E_{\text{c}} = E_{21} - E_{22} \tag{58}$$

Besides the above criteria, this study uses the cost per unit time (C_{tot}) to assess the economics of the system.

5. Results and Discussion

5.1 Model validation

In this part, as the combined system is proposed firstly, it is very difficult to verify the whole system. The feasible method is to verify the sub-cycles separately, and thus the reliability of the combined system is ensured. Table 3 lists the verification results of the current SCRC model with the model used in Refs. [18, 53]. Table 4 shows the results of the current KC model and the results given in Ref. [54] under the same input operation conditions. Table 5 shows the results of AARC in this study with Ref. [39] at the same condensation and evaporation pressure. It can be seen that the three sub-cycle models in this study are all reliable. Therefore, the combined cycle model can be also considered accurate.

5.2 Simulation results

In this study, the medium-temperature waste heat is from a Saturn 20 gas turbine unit produced by Solar company. The rated operating parameters are shown in Table 6. For this proposed system, the simulation program is developed using the assumed input conditions shown in Table 7. Table 8 lists the state parameters for each point of the exhaust and SCRC. The stream properties at each point of AARC and KC are shown in Table 9. Table 10 summarizes the calculated values of the performance indicators under the designed conditions.

Table 3 Comparison between the present study and those in other studies for the SCRC

Parameters	$T_{\min}$/°C	$T_{\max}$/°C	$P_{\max}$/MPa	PR	η_{MC} & η_{RC}/%	η_{t}/%	ε_{HTR}/%	E_{LTR}/%
	32	550	20.0	2.6	89	90	96.3	92.1
Results		Ref. [18]	Ref. [53]	Current model		Ref. [18]	Ref. [53]	Current model
	χ	0.4	0.41	0.402	η_{th}	45.27	45.27	45.09

Table 4 Model validation for the KC between the present work and Ref. [54]

Parameter	Ref. [54]	Current model
Pump II power/kW	5.20	5.22
Pump III power/kW	0.61	0.6084
Turbine II power/kW	260	259.7
KC net power/kW	254.19	253.8
KC thermal efficiency/%	22.25	22.17

Table 5 Validation results for the AARC system with Ref. [39]

Parameter	Ref. [39]	Current model
Poor solution concentration	0.3258	0.3308
Basic solution concentration	0.4258	0.4258
Rich solution concentration	0.9996	0.99
Rectifier exit mass flow/kg·s^{-1}	0.037 34	0.0373
Cooling capacity/kW	41.09	44.57
Absorption chiller COP	0.4804	0.4845

Table 6 Saturn 20 gas turbine performance parameters [55]

Parameters		Values
Output/kW		1210
Heat rate/kJ·kW^{-1}·h^{-1}		14 795
Unit efficiency/%		24.3
Flue gas flow/kg·h^{-1}		23 540
Exhaust temperature/°C		505
Unit size	*L*/m	6.7
	W/m	2.4
	H/m	2.7
Unit weight/kg		10 530

Table 7 Assumed input parameters for simulation

Terms	Values
Ambient temperature/°C	25
Ambient pressure/MPa	0.1013
SCRC low pressure/MPa	7.5
SCRC pressure ratio	3
Pinch point temperature difference, ΔT_{pinch}/°C	10
Approach point temperature difference $\Delta T_{approach}$/°C	8
Rectifier outlet ammonia concentration	0.99
Condensation pressure/MPa	1.042
Evaporation pressure/MPa	0.208
Evaporator outlet temperature/°C	–10
Isentropic efficiency of MC & RC, η_{MC} & η_{RC}	0.85
Isentropic efficiency of pumps, η_p	0.8
Isentropic efficiency of turbine I & turbine II, η_{turI} & η_{turII}	0.9
Effectiveness of HTR & LTR, ε_{HTR} & ε_{LTR}	0.82
Effectiveness of heater, ε_{heater}	0.86
Effectiveness of SHX, ε_{SHX}	0.8

Table 8 Thermodynamic properties at each state for the exhaust and SCRC

Cycle	State	*T*/ °C	*P*/MPa	*h*/ kJ·kg^{-1}	*s*/ kJ·kg^{-1}·K^{-1}	*m*/ kg·s^{-1}
Exhaust	w1	505	0.1013	–2318	8.088	6.539
	w2	347.6	0.1013	–2510	7.813	6.539
	w3	100	0.1013	–2796	7.225	6.539
SCRC	1	32	7.5	–144.1	–1.206	4.176
	2	93.46	22.5	–108.2	–1.192	4.176
	3a	243.2	22.5	142.6	–0.608	4.176
	3b	243.2	22.5	142.6	–0.608	2.363
	3	243.2	22.5	142.6	–0.608	6.609
	4	321.9	22.5	243.6	–0.4257	6.609
	5	475	22.5	433.4	–0.1418	6.609
	6	352.1	7.5	306.3	–0.119	6.609
	7	262.8	7.5	205.2	–0.2933	6.609
	8	123.9	7.5	46.78	–0.6361	6.609
	8a	123.9	7.5	46.78	–0.6361	4.176
	8b	123.9	7.5	46.78	–0.6361	2.363
	9	92.11	7.5	6.504	–0.7419	4.176

According to the state parameters listed in Table 8, the *T*-*s* diagram of SCRC is shown in Fig. 3. It can be found that the lowest point of the cycle (state 1) is very close to the critical point of carbon dioxide (*P*=7.3773 MPa, *T*= 31.98°C) [56]. Table 10 shows that the thermal efficiency of the combined cycle is 30.74%, and it can be calculated that the efficiency of the whole system (including the gas turbine) reaches 43.66%, which is 19.36% higher than the single gas turbine.

The exergy destruction ratio of each system component is shown in Fig. 4. It can be seen that HRVG is the component with the largest exergy destruction, followed by absorber III, LTR, cooler and regenerator III. Therefore, it can be concluded that the main exergy destruction is caused by the temperature differences in heat transfer progresses. However, the temperature difference is small in the heater because CO_2 and flue gas have similar specific heat changes and the heat exchange process will achieve a good match. The exergy destruction ratios of turbine I and turbine II are 8.13% and 6.8%, respectively, and the compressors' total exergy destruction reaches 7.01%. This kind of exergy destruction is mainly derived from the dissipation effect [57]. Therefore, to minimize the components' exergy destruction is one of the important ways for system performance improvement.

Table 9 Stream properties at each point of AARC and KC

Cycle	State	T/°C	P/MPa	h/kJ·kg^{-1}	s/kJ·kg^{-1}·K^{-1}	m/kg·s^{-1}	x
AARC	10	35	0.208	–65.75	0.4011	0.5367	0.373
	11	35.11	1.042	–64.55	0.4018	0.5367	0.373
	12	86.86	1.042	164.7	1.089	0.5367	0.373
	13	110.3	1.042	301.5	1.407	0.4651	0.278
	14	50.15	1.042	36.99	0.6574	0.4651	0.278
	15	50.31	0.208	36.99	0.6603	0.4651	0.278
	16	105.1	1.042	1546	5.072	0.075 73	0.9564
	17	89.4	1.042	176.6	1.122	0.004 124	0.373
	18	66.66	1.042	1408	4.693	0.071 61	0.99
	19	26.57	1.042	117.8	0.4526	0.071 61	0.99
	20	5.561	1.042	18.79	0.1098	0.071 61	0.99
	21	–17.72	0.208	18.79	0.1307	0.071 61	0.99
	22	–10	0.208	1208	4.753	0.071 61	0.99
	23	16.57	0.208	1307	5.112	0.071 61	0.99
KC	24	35	0.5961	–75.17	0.3682	0.7663	0.5731
	25	35.86	5.558	–67.32	0.3732	0.7663	0.5731
	26	43.92	5.558	–30.83	0.4898	0.7663	0.5731
	27	317.6	5.558	2413	5.97	0.7663	0.5731
	28	99.66	0.2408	1854	6.134	0.7663	0.5731
	29	61.87	0.2408	750.4	3.057	0.7663	0.5731
	30	47.13	0.2408	146	1.081	5.127	0.3961
	31	35	0.2408	–71.77	0.3912	5.127	0.3961
	32	35.05	0.5961	–71.26	0.3916	5.127	0.3961
	32a	35.05	0.5961	–71.26	0.3916	0.5303	0.3961
	32b	35.05	0.5961	–71.26	0.3916	4.596	0.3961
	33	45.68	0.5961	–24.51	0.5407	4.596	0.3961
	34	69.66	0.5961	159.5	1.089	4.596	0.3961
	35	69.66	0.5961	89.11	0.8722	4.361	0.365
	36	58.51	0.5961	39.83	0.7261	4.361	0.365
	37	44.97	0.2408	39.83	0.7313	4.361	0.365
	38	69.66	0.5961	1460	5.099	0.236	0.971
	39	51.92	0.5961	1342	4.745	0.236	0.971

* The enthalpy and entropy of the triple point state of water are both 0.

Table 10 Performance calculation results of the combined system

Terms	Values	Terms	Values
Power consumption of MC/kW	150	Cooling capacity/kW	85.14
Power consumption of RC/kW	233.1	SCRC thermal efficiency/%	36.45
Power consumption of pump I/kW	0.6471	KC thermal efficiency/%	22.39
Power consumption of pump II/kW	6.01	Absorption chiller COP	0.5042
Power consumption of pump III/kW	2.658	Thermal efficiency/%	30.74
Power generated by turbine I/kW	840.3	Exergy efficiency/%	61.55
Power generated by turbine II/kW	428	Cost per unit time/USD·h^{-1}	4.858
Net power output/kW	876		

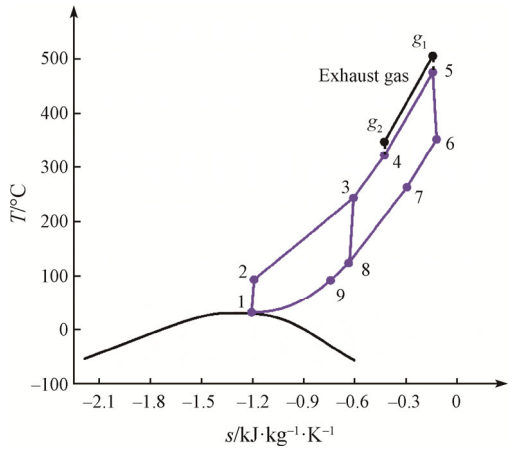

Fig. 3 *T-s* diagram of SCRC

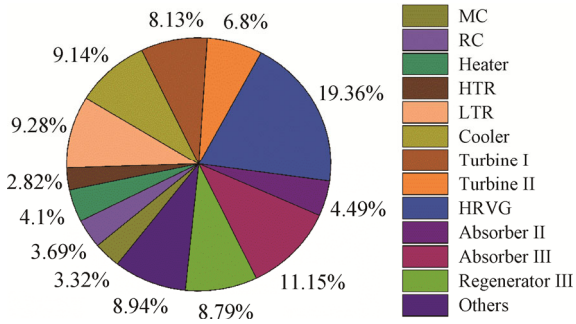

Fig. 4 Exergy destruction distribution in the system

5.3 Parametric analysis

In this section, the effects of some key parameters, such as the compressor inlet pressure (P_1), the SCRC pressure ratio (PR), the main compressor inlet temperature (T_1), the turbine I inlet temperature (T_5), and the AARC generator pressure (P_{gen}), are selected to investigate the thermodynamic and economic performances of the combined SCRC/AARC/KC system. Note that the system is still assumed to recover Saturn 20 gas turbine waste heat, and when one of the parameters is varied, the others remain unchanged.

5.3.1 Effects of the compressor inlet pressure

The compressor inlet pressure (P_1) will have an influence on the performance not only of the top SCRC, but also of the KC and the bottom AARC. Therefore, it is necessary to study the impact of this parameter on system performance in detail. Assuming the SCRC cycle with high pressure of 27.0 MPa, the effects of P_1 on system performance are respectively shown in Figs. 5–6.

Fig. 5(a) shows the changes of the recompression ratio (χ), the working fluid flow rates into turbine I (m_5), MC (m_{8a}) and RC (m_{8b}), power generated by turbine I (W_{turI}) and power consumption of the compressors (ΣW_{comp}) in top SCRC. It is observed that when the pressure is lower than about 7.6 MPa, the curves change very sharply, especially χ and ΣW_{comp}. That is mainly because the CO_2 properties change very sharply near the critical point. As shown in Fig. 5(a), the recompression ratio increases firstly and then decreases after the pressure exceeds about 7.6 MPa, which leads to the opposite trend of m_{8a} and m_{8b}. And as the compressor inlet pressure increases, the compression ratio is reduced and it leads to decreases of ΣW_{comp} and W_{turI}. Fig. 5(b) illustrates the effects of P_1 on the SCRC net power output ($W_{net,SCRC}$), the KC net power output ($W_{net,KC}$), the net power output (W_{net}) and the refrigeration output (Q_c) of the combined system. When P_1 increases, $W_{net,SCRC}$ rises firstly and then keeps almost unchanged. The reason is that ΣW_{comp} decreases more than W_{turI} at the beginning and then the degree of their declines is almost the same which has been shown in Fig. 5(a). With the increase of P_1, the outlet temperature of MC and RC (T_2 and T_{3b}) both decrease, that will result in a temperature reduction of CO_2 after the heat recovery completion (T_4). Therefore, the heat exchange load in the heater increases, which in turn causes a drop of heat absorption into KC, and thus leads to a decrease of $W_{net,KC}$. However, when the physical properties change of CO_2 tends to be stable, this effect

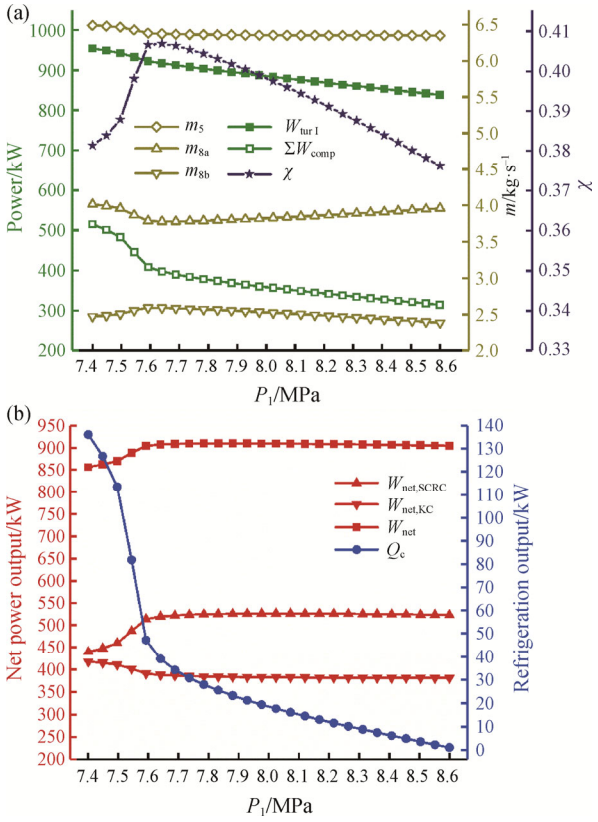

Fig. 5 Effects of P_1 on the system performance (a) m, χ, W_{turI}, ΣW_{comp} (b) W, Q_c

becomes less obvious, and thus the net power output of the combined system also remains basically unchanged. Furthermore, a decrease in compressor outlet temperature causes a decrease in the generator inlet temperature (T_{8a}), resulting in a heat reduction entering the bottom AARC. Because the refrigeration output is relatively small compared to the net power output, the drop of Q_c is more obvious, especially in the stage of drastic changes of CO_2 properties.

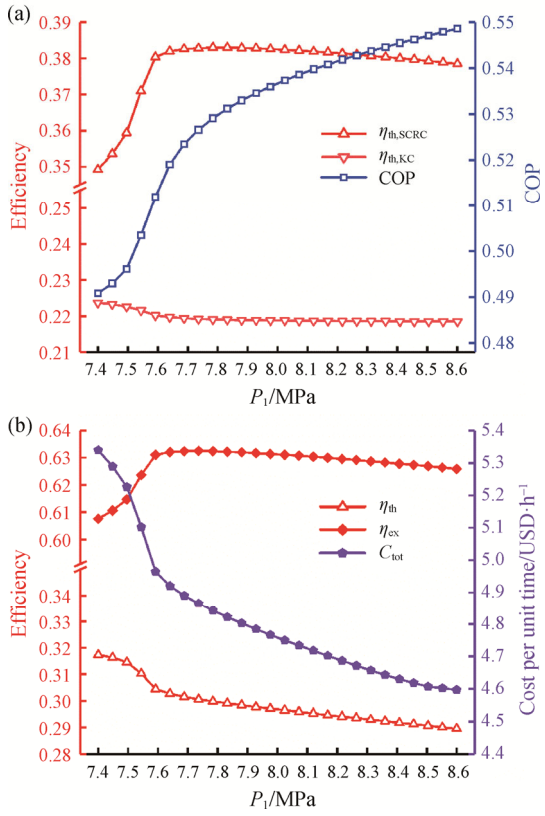

Fig. 6 Effects of P_1 on the system performance (a) $\eta_{th,SCRC}$, $\eta_{th,KC}$, COP (b) η_{th}, η_{ex}, C_{tot}

The changes of the SCRC thermal efficiency ($\eta_{th,SCRC}$), the KC thermal efficiency ($\eta_{th,KC}$) and the absorption chiller COP (COP) with an increase of the compressor inlet pressure are shown in Fig. 6(a), and changes of the thermal efficiency (η_{th}), the exergy efficiency (η_{ex}) and the cost per unit time (C_{tot}) of the combined system are illustrated in Fig. 6(b). As discussed before, as the heat added into SCRC increases but that into KC decreases, the changes of $W_{net,SCRC}$ and $W_{net,KC}$ show the opposite trends as shown in Fig. 5(b). Therefore, it can be known that $\eta_{th,SCRC}$ will increase first and then decrease, and $\eta_{th,KC}$ will decrease first and then tend to be stable. In addition, the absorption chiller COP increases while the refrigeration output has a decrease. When P_1 changes around the critical pressure, η_{th} and η_{ex} show the opposite changing trends. That is because the decline of refrigeration output is much greater than the decline of refrigeration exergy output. When P_1 continues to increase, both η_{th} and η_{ex} drop because the decrease of refrigeration output is dominant. In addition, the main reason for the decline of C_{tot} is that the decrease of power consumption and power generation in SCRC reduces the costs for purchasing the compressors and turbine I.

5.3.2 Effects of the SCRC pressure ratio

The pressure ratio is a very important parameter which can not only affect the amount of the compression power and the turbine I power, but also affect the heat exchange capacity of HTR and LTR, thus having an impact on the system efficiency and economic performance of the combined system. Limited by the ability of the material to withstand pressure at high temperatures, the pressure ratio cannot be too high, so the range of the value is set from 2.5 to 4.15 with a cycle low pressure of 7.5 MPa.

As shown in Fig. 7(a), it can be known that although the working fluid flow rates entering turbine I and MC both reduced, the power generation or power consumption by the unit mass working fluid is greatly

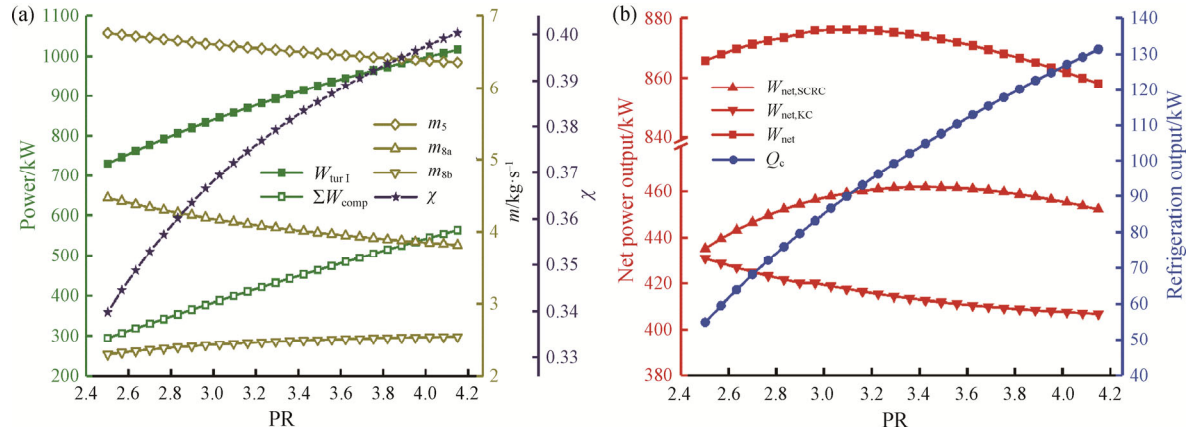

Fig. 7 Effects of PR on the system performance (a) m, χ, W_{turI}, ΣW_{comp} (b) W, Q_c

improved with an increase of PR, so the turbine I power output and the compressors power consumption both increase. The reason why $W_{net,SCRC}$ rises at first as shown in Fig. 7(b) can be explained that the power generation increases rapidly than the power consumption at first, otherwise $W_{net,SCRC}$ will have a decrease, and its maximum value is 461.9 kW when PR equals to 3.425. Furthermore, an increase in PR will cause the turbine I outlet temperature (T_6) and the heater inlet temperature (T_4) to drop, which will increase the heat absorption into the heater but decrease the heat transfer load in HRVG, resulting in a decline of the KC net power output. When the increase of $W_{net,SCRC}$ is greater than the decrease of $W_{net,KC}$, the net power output will increase. That means there exists a maximum value of W_{net} which is found to be 875.7 kW obtained at PR=3.227. In addition, as PR increases, the main compressor outlet temperature (T_2) rises, and the heat transferred to the bottom AARC increases due to more heat absorption into the top SCRC and less heat load in HTR and LTR. Therefore, the refrigeration output will rise with the increase of PR.

Fig. 8 shows the effects of the pressure ratio on efficiency, COP, and the cost per unit time. As shown in Fig. 8(a), the SCRC thermal efficiency shows the same trend with $W_{net,SCRC}$. The KC thermal efficiency drops slightly, and the reason is the ammonia-water temperature at the outlet of HRVG (T_{27}) has a slight decrease for its heat load reduction which has been analyzed before. COP also decreases, which is opposite to the change of Q_c. As shown in Fig. 8(b), the combined cycle thermal efficiency keeps increasing with the increase of PR, but the exergy efficiency increases first and then decreases. The reason is that the increasing degree of Q_c is bigger than the decreasing degree of W_{net} but the increasing degree of E_c is smaller than that of W_{net} after W_{net} reaching its maximum value. The maximum exergy efficiency is 61.65% when PR is equal to 3.293. In addition, the cost per unit time keeps rising with the increase of PR. This is mainly due to the significant increase in the purchase costs of compressors and turbine I.

5.3.3 Effects of the main compressor inlet temperature

Fig. 9(a) shows that with the increase of the main compressor inlet temperature, the recompression ratio drops, and the CO_2 flow rates entering turbine I and MC increase but the flow rate through RC decreases. With a

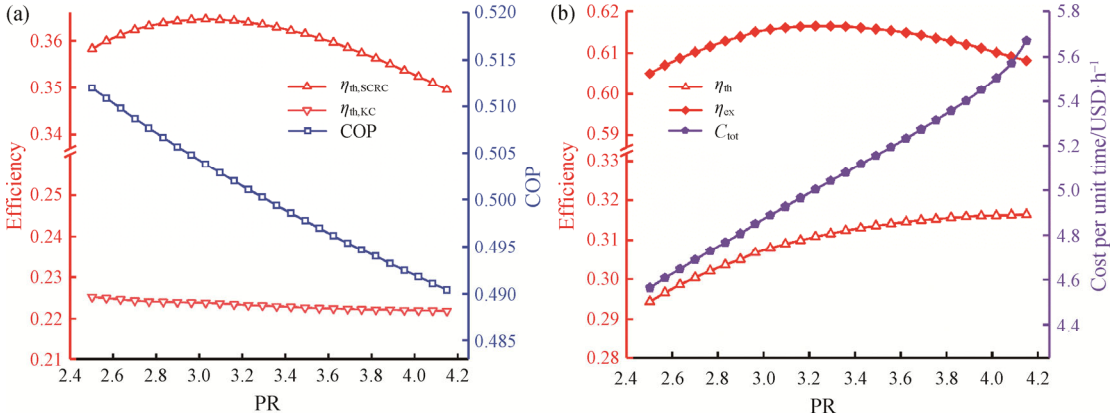

Fig. 8 Effects of PR on the system performance (a) $\eta_{th,SCRC}$, $\eta_{th,KC}$, COP (b) η_{th}, η_{ex}, C_{tot}

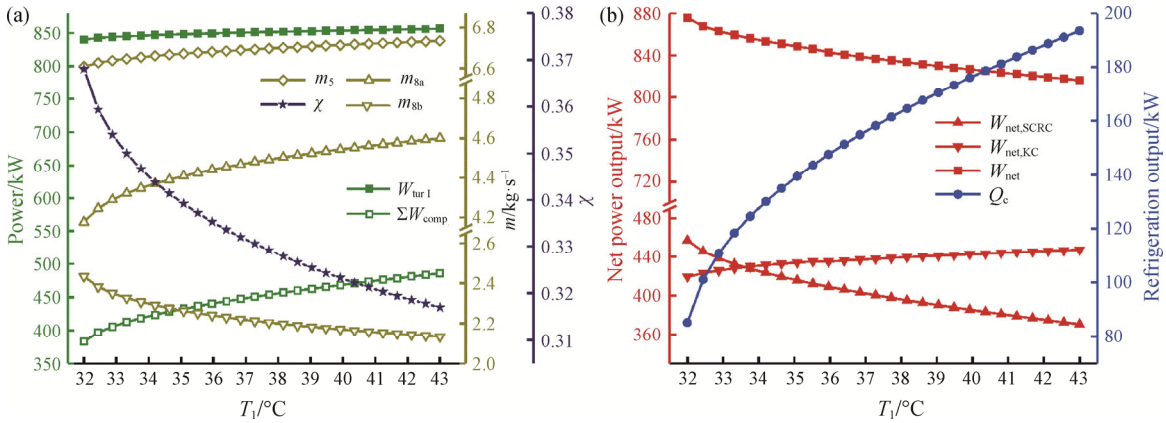

Fig. 9 Effects of T_1 on the system performance (a) m, χ, W_{turI}, ΣW_{comp} (b) W, Q_c

constant pressure ratio, an increase of main compressor inlet temperature will cause a decrease in compression power consumption, and the reduction of turbine I power output is not obvious due to that the increase of m_5 is not much. Therefore, the SCRC net power output will decrease as T_1 rises. From Fig. 9(b), when T_1 rises from 32°C to 43°C, the KC net power output increases from 419.4 kW to 447.3 kW and the refrigeration output rises by 108.46 kW from 85.14 kW to 193.6 kW. That is because the increase of T_1 will lead to an increase of the outlet temperature of MC (T_2), and result in the temperature of CO_2 entering the heater (T_4) and out of LTR (T_8) to rise, thus leading to an increase in heat transfer load both in HRVG and the generator. Besides, the increase of heat absorption into AARC is greater than that into KC in this system, so Q_c increases more obviously than $W_{net,KC}$. Moreover, the reason why the net power output drops is that the decrease of $W_{net,SCRC}$ is greater than the increase of $W_{net,KC}$.

From Fig. 10(a), it is observed that with the increase of T_1, the SCRC thermal efficiency and COP both decrease, and the KC thermal efficiency basically remains unchanged. By considering the discussion in Fig. 9(b), it is known that the compressor inlet temperature mainly has an influence on the top SCRC and the bottom AARC, but little on the KC. In Fig. 10(b), the thermal efficiency increases but the exergy efficiency decreases, that reflects the inequality of Q_c and E_c, although the total energy output is increased, but the total exergy output is reduced. With an increase of T_1, the economics becomes worse due to more equipment cost required in the bottom AARC.

5.3.4 Effects of the turbine I inlet temperature

The turbine I inlet temperature is also an important influencing factor in the system. With an increase of turbine I inlet temperature, Figs. 11–12 analyze the changes of the same performance parameters as those done previously.

As shown in Fig. 11(a), the CO_2 flow rates respectively into turbine I, MC and RC, and the recompression ratio, the compression and turbine I power all decrease when T_5 increases. Fig. 11(b) indicates that when the temperature rises from 395°C to 495°C, the SCRC net power output decreases for the reason that the compression power drops greater than the turbine I power. And it can be observed that the refrigeration output decreases while the KC net power output increases. This is mainly due to that the reduction of m_5 leads to a decline of heat absorption into SCRC, thus leading to less

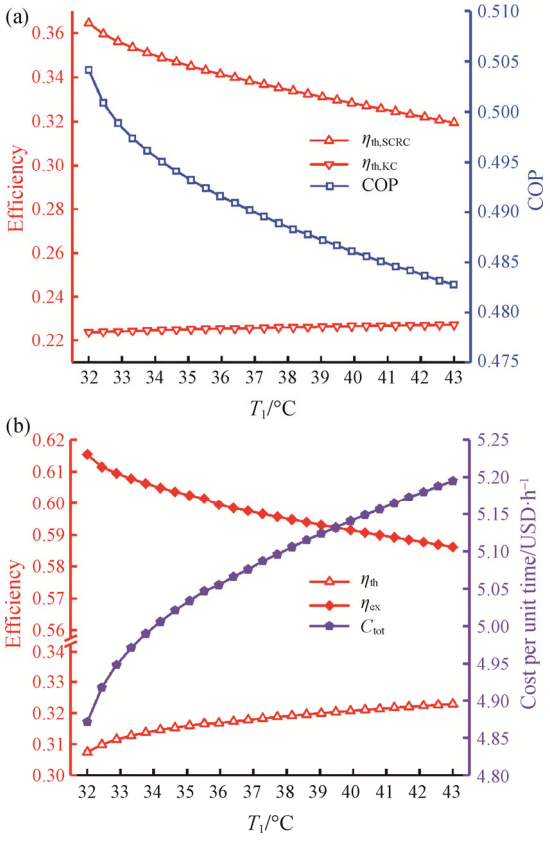

Fig. 10 Effects of T_1 on the system performance (a) $\eta_{th,SCRC}$, $\eta_{th,KC}$, COP (b) η_{th}, η_{ex}, C_{tot}

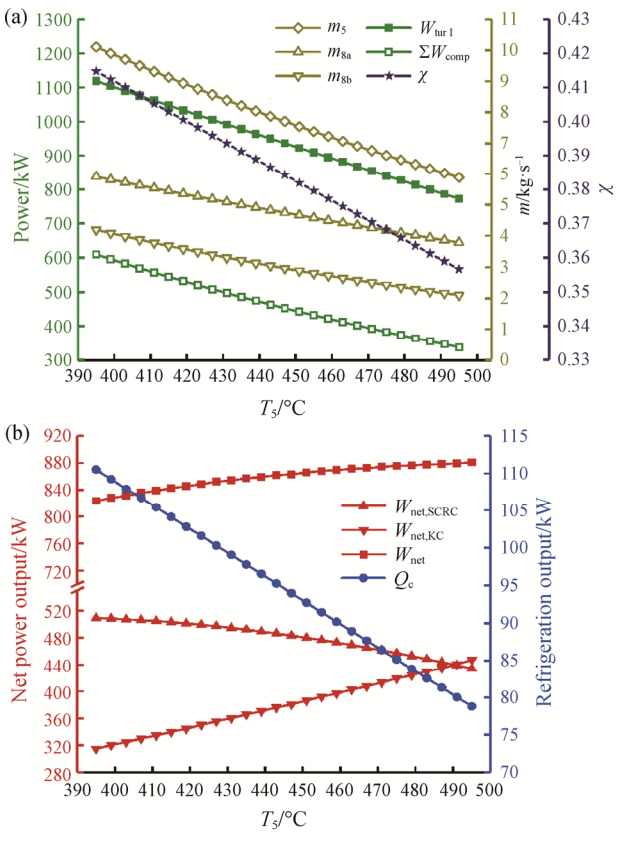

Fig. 11 Effects of T_5 on the system performance (a) m, χ, W_{turI}, ΣW_{comp} (b) W, Q_c

heat entering AARC and more heat entering KC. The total net power output has an increase as T_5 rises, which is mainly because the increase of $W_{net,KC}$ is more dominant than the decrease of $W_{net,SCRC}$.

Fig. 12 illustrates the effects of the turbine I inlet temperature on efficiencies, COP, and the cost per unit time. As shown in Fig. 12(a), the absorption chiller COP has a slight decrease while $\eta_{th,SCRC}$ and $\eta_{th,KC}$ both have relatively significant improvements. It has been known that HRVG heat transfer load increases as T_5 rises, so the turbine II inlet temperature (T_{27}) also has an increase, which will enhance the ability of working fluids in power generation, leading to the increase of $\eta_{th,SCRC}$ and $\eta_{th,KC}$. In addition, although Q_c and E_c both decrease, the growth of net power output is dominant, therefore, η_{th} and η_{ex} both rise as shown in Fig. 12(b). Furthermore, the cost per unit time is reduced with the increase of T_5, which means for this combined system, trying to improve T_5 is benefit not only for efficiencies, but also for economics.

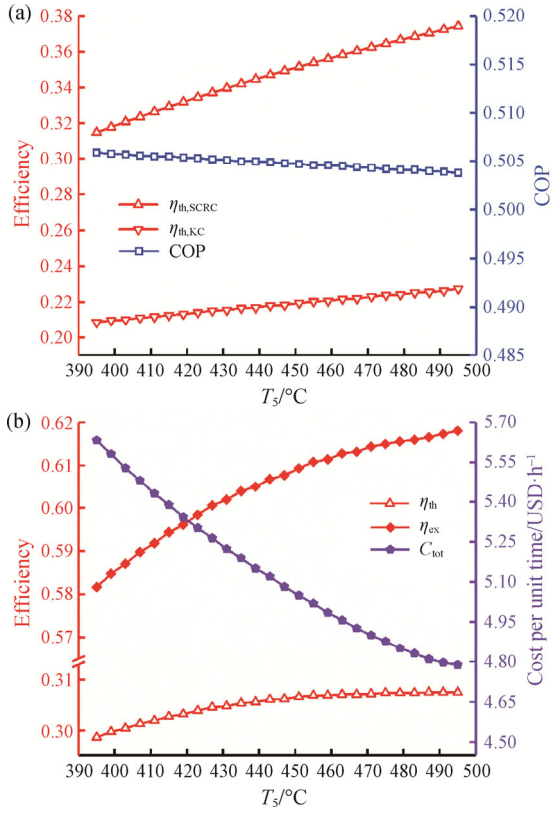

Fig. 12 Effects of T_5 on the system performance (a) $\eta_{th,SCRC}$, $\eta_{th,KC}$, COP (b) η_{th}, η_{ex}, C_{tot}

5.3.5 Effects of the AARC generator pressure

Fig. 13 shows the effects of AARC generator pressure on system performance. With an increase of P_{gen}, the absorption chiller COP decreases, and the heat transferred into the generator will decline with the previous system assumptions. Therefore, the refrigeration output will decrease while the net power output will not be affected by the parameters change of the bottom cycle. So the increase of P_{gen} leads to the reduction of the thermal system efficiency and exergy efficiency. Moreover, the cost per unit time also decreases due to less cost for the AARC equipment.

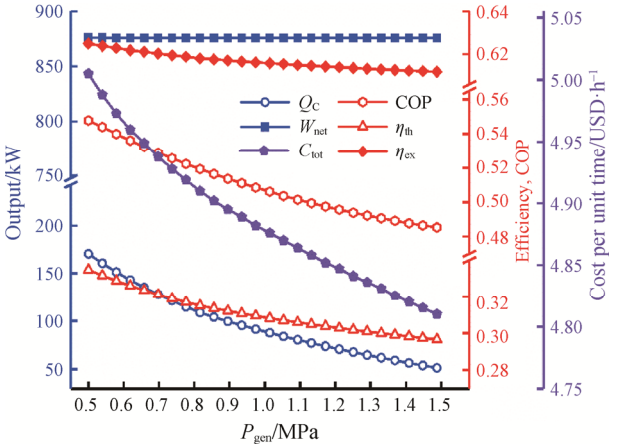

Fig. 13 Effects of P_{gen} on the system performance Q_c, W_{net}, COP, η_{th}, η_{ex}, and C_{tot}

6. Conclusions

Based on energy cascade utilization, a novel cogeneration system integrated with a SCRC system, an AARC system and a KC system is proposed and investigated for efficient recovery and conversion of medium-temperature waste heat. The steady-state mathematical model is built first, and then a detailed parametric analysis is carried out to examine the impacts of some key parameters on the system performance. The main conclusions drawn from this study are listed as follows:

(1) When the exhaust heat is 505°C from a gas turbine, the thermal efficiency and exergy efficiency of the combined system reach 30.74% and 61.55% under designed conditions, respectively, and the cost per unit time is about 4.858 USD/h.

(2) The main exergy destruction of the combined system is derived from the temperature differences in heat transfer progresses, and the largest exergy destruction occurs in the HRVG which accounts for 19.36% of the total.

(3) Increasing the SCRC pressure ratio, the main compressor inlet temperature and the turbine I inlet temperature have a positive effect on the first law efficiency of the system, but increasing the compressor inlet pressure and the AARC generator pressure do the opposite, respectively.

(4) When changing a key parameter, the changing trends of capital cost and thermal efficiency are always

the same except for the turbine I inlet temperature, so trying to increase turbine I inlet temperature is beneficial not only for thermal performance, but also for economic performance.

Acknowledgements

This work was supported by the Shandong Provincial Natural Science Foundation of China (No. ZR2019MEE045), the National Natural Science Foundation of China (No. 51776203) and the Key Project of National Natural Science Foundation of China (No. 61733010).

References

[1] Li C.Y., Wang H.X., Power cycles for waste heat recovery from medium to high temperature flue gas sources - from a view of thermodynamic optimization. Applied Energy, 2016, 180: 707–721.

[2] Danish S.N., Waste heat recovery from heavy-duty diesel engine exhaust gases by medium temperature ORC system. Science China (Technological Sciences), 2011, 54(10): 2746–2753.

[3] Utlu Z., Investigation of the potential for heat recovery at low, medium, and high stages in the Turkish industrial sector (TIS): An application. Energy, 2015, 81: 394–405.

[4] Su R.Z., Yu Z.T., Xia L., Sun J.N., Performance analysis and multi-objective optimization of an integrated gas turbine/supercritical CO_2 recompression/transcritial CO_2 cogeneration system using liquefied natural gas cold energy. Energy Conversion and Management, 2020, 220: 113136.

[5] Sadreddini A., Ashjari M.A., Fani M., Mohammadi A., Thermodynamic analysis of a new cascade ORC and transcritical CO_2 cycle to recover energy from medium temperature heat source and liquefied natural gas. Energy Conversion and Management, 2018, 167: 9–20.

[6] Mohtaram S., Chen W., Zargar T., Lin J., Energy-exergy analysis of compressor pressure ratio effects on thermodynamic performance of ammonia water combined cycle. Energy Conversion and Management, 2017, 134: 77–87.

[7] Mohtaram S., Lin J., Chen W., Nikbakht M.A., Evaluating the effect of ammonia-water dilution pressure and its density on thermodynamic performance of combined cycles by the energy-exergy analysis approach. Mechanics, 2017, 23(2): 209–219.

[8] Zhang X.J., Wu L.J., Wang X.L., Ju G.D., Comparative study of waste heat steam SRC, ORC and S-ORC power generation systems in mediumlow temperature. Applied Thermal Engineering, 2016, 106: 1427–1439.

[9] Ebrahimi M., Majidi S., Exergy-energy-environ evaluation of combined cooling heating and power system based on a double stage compression regenerative gas turbine in large scales. Energy Conversion and Management, 2017, 150: 122–133.

[10] Cao Y., Dai Y.P., Comparative analysis on off-design performance of a gas turbine and ORC combined cycle under different operation approaches. Energy Conversion and Management, 2017, 135: 84–100.

[11] Tchanche B.F., Lambrinos G., Frangoudakis A., Papadakis G., Low-grade heat conversion into power using organic Rankine cycles – A review of various applications. Renewable and Sustainable Energy Reviews, 2011, 15(8): 3963–3979.

[12] Li H., Yang Y., Cheng Z.Y., Sang Y.Q., Dai Y.P., Study on off-design performance of transcritical CO_2 power cycle for the utilization of geothermal energy. Geothermics, 2018, 71: 369–379.

[13] Yari M., Mehr A.S., Zare V., Mahmoudi S.M.S., Rosen M.A., Exergoeconomic comparison of TLC (trilateral Rankine cycle), ORC (organic Rankine cycle) and Kalina cycle using a low grade heat source. Energy, 2015, 83: 712–722.

[14] Zhang X.X., He M.G., Zhang Y., A review of research on the Kalina cycle. Renewable and Sustainable Energy Reviews, 2015, 16(7): 5309–5318.

[15] Abram T., Ion S., Generation-IV nuclear power: A review of the state of the science. Energy Policy, 2008, 36(12): 4323–4330.

[16] Osorio J.D., Hovsapian R., Ordonez J.C., Effect of multi-tank thermal energy storage, recuperator effectiveness, and solar receiver conductance on the performance of a concentrated solar supercritical CO_2-based power plant operating under different seasonal conditions. Energy, 2016, 115: 353–368.

[17] Ahn Y., Bae S.J., Kim M., Cho S.K., Baik S., Lee J.I., Cha J.E., Review of supercritical CO_2 power cycle technology and current status of research and development. Nuclear Engineering and Technology, 2015, 47(6): 647–661.

[18] Sarkar J., Second law analysis of supercritical CO_2 recompression Brayton cycle. Energy, 2009, 34(9): 1172–1178.

[19] Sarkar J., Bhattacharyya S., Optimization of recompression S-CO_2 power cycle with reheating. Energy Conversion and Management, 2009, 50(8): 1939–1945.

[20] Ma Y.G., Zhang X.W., Liu M., Yan J.J., Liu J.P., Proposal and assessment of a novel supercritical CO_2 Brayton cycle integrated with LiBr absorption chiller for concentrated solar power applications. Energy, 2018, 148: 839–854.

[21] Wang X.R., Yang Y., Zhang Y., Dai Y.P., Exergy and exergoeconomic analyses of a supercritical CO_2 cycle for

a cogeneration application. Energy, 2017, 119: 971–982.

[22] Hou S.Y., Cao S., Yu L.J., Zhou Y.D., Wu Y.D., Zhang F.Y., Performance optimization of combined supercritical CO_2 recompression cycle and regenerative organic Rankine cycle using zeotropic mixture fluid. Energy Conversion and Management, 2018, 166: 187–200.

[23] Li H., Wang M.K., Wang J.Y., Dai Y.P., Exergoeconomic analysis and optimization of a supercritical CO_2 cycle coupled with a Kalina cycle. Journal of Energy Engineering, 2017, 143(2): 04016055.

[24] Wu C., Wang S.S., Feng X.J., Li J., Energy, exergy and exergoeconomic analyses of a combined supercritical CO_2 recompression Brayton/absorption refrigeration cycle. Energy Conversion and Management, 2017, 148: 360–377.

[25] Li H., Su W., Cao L.Y., Chang F., Xia W.K., Dai Y.P., Preliminary conceptual design and thermodynamic comparative study on vapor absorption refrigeration cycles integrated with a supercritical CO_2 power cycle. Energy Conversion and Management, 2018, 161: 162–171.

[26] Hassan H.Z., Mohamad A.A., A review on solar cold production through absorption technology. Renewable and Sustainable Energy Reviews, 2012, 16(7): 5331–5348.

[27] Garousi Farshi L., Mahmoudi S.M.S., Rosen M.A., Yari M., Amidpour M., Exergoeconomic analysis of double effect absorption refrigeration systems. Energy Conversion and Management, 2013, 65: 13–25.

[28] Kalina A.I., Combined-cycle system with novel bottoming cycle. Journal of Engineering for Gas Turbines and Power, 1984, 106: 737–742.

[29] Larsen U., Nguyen T.V., Knudsen T., Haglind F., System analysis and optimisation of a Kalina split-cycle for waste heat recovery on large marine diesel engines. Energy, 2014, 64: 484–494.

[30] Yu Z.T., Su R.Z., Feng C.Y., Thermodynamic analysis and multi-objective optimization of a novel power generation system driven by geothermal energy. Energy, 2020, 199: 117381.

[31] Cao L.Y., Wang J.F., Dai Y.P., Thermodynamic analysis of a biomass-fired Kalina cycle with regenerative heater. Energy, 2014, 77: 760–770.

[32] Li S.L., Dai Y.P., Thermo-economic comparison of Kalina and CO_2 transcritical power cycle for low temperature geothermal sources in China. Applied Thermal Engineering, 2014, 70(1): 139–152.

[33] Campos Rodríguez C.E., Escobar Palacio J.C., Venturini O.J., Silva Lora E.E., Cobas V.M., Marques dos Santos D., et al., Exergetic and economic comparison of ORC and Kalina cycle for low temperature enhanced geothermal system in Brazil. Applied Thermal Engineering, 2013, 52: 109–119.

[34] Bombarda P., Invernizzi C.M., Pietra C., Heat recovery from Diesel engines: A thermodynamic comparison between Kalina and ORC cycles. Applied Thermal Engineering, 2010, 30(2–3): 212–219.

[35] Jonsson M., Yan J., Exergy and pinch analysis of diesel engine bottoming cycles with ammonia-water mixtures as working fluid. International Journal of Thermodynamics, 2000, 3(2): 57–71.

[36] Kato Y., Nitawaki T., Muto Y., Medium temperature carbon dioxide gas turbine reactor. Nuclear Engineering and Design, 2004, 230(1): 195–207.

[37] Li X.J., Zhang X.R., Component exergy analysis of solar powered transcritical CO_2 Rankine cycle system. Journal of Thermal Science, 2011, 20(03): 195–200.

[38] Kim Y.M., Kim C.G., Favrat D., Transcritical or supercritical CO_2 cycles using both low- and high-temperature heat sources. Energy, 2012, 43(1): 402–415.

[39] Tian M.L., Yu Z.T., Zhao H.X., Yin J.Q., Thermodynamic analysis of an integrated solid oxide fuel cell, Organic Rankine Cycle and absorption chiller trigeneration system with CO_2 capture. Energy Conversion and Management, 2018, 171: 350–360.

[40] Zhu F.L., Chen L.G., Wang W.H., Thermodynamic analysis and optimization of an irreversible Maisotsenko-Diesel cycle. Journal of Thermal Science, 2019, 28(4): 659–668.

[41] Sun F., Ikegami Y., Jia B., A study on Kalina solar system with an auxiliary superheater. Renewable Energy, 2012, 41: 210–219.

[42] Yan Z.Q., Zhao P., Wang J.F., Dai Y.P., Thermodynamic analysis of an SOFC-GT-ORC integrated power system with liquefied natural gas as heat sink. International Journal of Hydrogen Energy, 2013, 38(8): 3352–3363.

[43] Yin J.Q., Yu Z.T., Zhang C.H., Tian M.L., Han J.T., Thermodynamic analysis of a novel combined cooling and power system driven by low-grade heat sources. Energy, 2018, 156: 319–327.

[44] Carneiro M.L.N.M., Gomes M.S.P., Energy, exergy, environmental and economic analysis of hybrid waste-to-energy plants. Energy Conversion and Management, 2019, 179: 397–417.

[45] Yin J.Q., Yu Z.T., Zhang C.H., Tian M.L., Han J.T., Thermodynamic analysis and multi-objective optimization of a novel power/cooling cogeneration system for low-grade heat sources. Energy Conversion and Management, 2018, 166: 64–73.

[46] Akbari Kordlar M., Mahmoudi S.M.S., Exergeoconomic analysis and optimization of a novel cogeneration system producing power and refrigeration. Energy Conversion and Management, 2017, 134: 208–220.

[47] Kwon K., Jeong S., Effect of vapor flow on the falling-film heat and mass transfer of the ammonia/water absorber. International Journal of Refrigeration, 2004, 27(8): 955–964.

[48] Khani L., Mahmoudi S.M.S., Chitsaz A., Rosen M.A., Energy and exergoeconomic evaluation of a new power/cooling cogeneration system based on a solid oxide fuel cell. Energy, 2016, 94: 64–77.

[49] Zare V., Mahmoudi S.M.S., Yari M., Amidpour M., Thermoeconomic analysis and optimization of an ammonia-water power/cooling cogeneration cycle. Energy, 2012, 47(1): 271–283.

[50] El-Emam R.S., Dincer I., Exergy and exergoeconomic analyses and optimization of geothermal organic Rankine cycle. Applied Thermal Engineering, 2013, 59(1): 435–444.

[51] Huang W.G., Wang J.F., Xia J.X., Zhao P., Dai Y.P., Performance analysis and optimization of a combined cooling and power system using low boiling point working fluid driven by engine waste heat. Energy Conversion and Management, 2019, 180: 962–976.

[52] Bejan A., Tsatsaronis G., Moran M., Thermal design and optimization. John Wiley & Sons, Inc, New York, 1996.

[53] Dostal V., Driscoll M.J., Hejzlar P., A supercritical carbon dioxide cycle for next generation nuclear reactors. PhD thesis. Department of Nuclear Engineering, Massachusetts Institute of Technology, USA, 2004.

[54] Wang J.F., Yan Z.Q., Ma S.L., Dai Y.P., Thermodynamic analysis of an integrated power generation system driven by solid oxide fuel cell. International Journal of Hydrogen, Energy, 2012, 37(3): 2535–2545.

[55] Solar Turbines, Gas Turbine Ratings, https://www.solarturbines.com/en_US/products/turbine-ratings.html; 2020. (accessed 27 February 2020)

[56] Li Y.X., Yu J.L., Thermodynamic analysis of a modified ejector-expansion refrigeration cycle with hot vapor bypass. Journal of Thermal Science, 2019, 28(4): 695–704.

[57] Seyitoglu S.S., Dincer I., Kilicarslan A., Energy and exergy analyses of hydrogen production by coal gasification. International Journal of Hydrogen Energy, 2017, 42(4): 2592–2600.